Hertel, D., **Schlink, U.** (2019):
Decomposition of urban temperatures for targeted climate change adaptation
Environ. Modell. Softw. **113** , 20 – 29

http://dx.doi.org/10.1016/j.envsoft.2018.11.015

Decomposition of urban temperatures for targeted climate change adaptation

Daniel Hertel[a,*], Uwe Schlink[a]

[a] *Department of Urban and Environmental Sociology, Helmholtz Centre for Environmental Research - UFZ, Permoserstraße 15, D-04318 Leipzig, Germany*

Abstract

A decomposition of the urban heat island (UHI) intensity (ΔT) into its contributing processes is suggested for the neighbourhood scale. The approach translates individual terms of the energy balance (radiation, evapotranspiration, heat storage, and convection) into temperature increments. It is exemplified using micrometeorological simulations (ENVI-met) for the quarter "Bayerischer Bahnhof" in Leipzig, Germany, under different wind conditions. In result heat storage and convection provide the principal contributions to UHI. The mapping of ΔT-contributions in a neighbourhood is a new tool facilitating the development of tailored measures for reduction of and adaptation to urban heat. For instance, the respective ΔT-contributions within a courtyard were -6.8 K, -2.6 K, -9.2 K and 15.7 K showing the mutual compensation effect which can be enhanced if suitable measures will be taken into action. At each individual location, considering the trade-offs of all ΔT-contributions can support a cost-benefit analysis creating optimal recommendations for city planners.

Keywords: Urban heat island, ENVI-met, climate adaptation, Leipzig

*Corresponding author. Tel.: +49 341 235 1704; Fax: +49 341 235 45 1704
Email address: `daniel.hertel@ufz.de` (Daniel Hertel)

1. Introduction

The urban heat island (UHI) effect, where urban areas have higher temperatures than the rural surrounding, embodies one of the most significant human-induced alterations to Earth's surface climate (Zhao et al., 2014). The modifications comprise changes in meteorological variables such as moisture availability (e.g.: Lee, 1991; Kuttler et al., 2007; Sailor, 2011) and urban - rural water vapour differences (Holmer & Eliasson, 1999), temperature (e.g.: Arnfield, 2003), heat fluxes (e.g.: Grimmond & Oke, 2002) and turbulence (e.g.: Roth, 2000; Arnfield, 2003). Given this UHI phenomenon and the observed increase in frequency and persistence of heat waves in european cities after 1997 (e.g.: Christidis et al., 2015; Morabito et al., 2017), there is urgent need for heat mitigation and adaptation actions. The development of targeted strategies requires knowledge about the local UHI structures in order to minimise costs and efforts, maximise heat reduction and avoid adverse health effects on the inhabitants. We define the UHI effect as surface temperature difference between an urban region and the same area without built-up structures. With this local UHI intensity ΔT we can assess excess heat directly on a scale where adaptation is needed, namely within the living environment of urban residents.

So far, small-scale spatio-temporal variability of $\Delta T(\mathbf{x}, t)$ in space ($\mathbf{x}$) and time (t) has been hardly examined by observations at the neighbourhood scale, because a sufficient density of measurements is very expensive and difficult to realise. Micrometeorological models, such as MISKAM (Eichhorn, J., 2011), MUKLIMO (Sievers & Zdunkowski, 1986; Sievers, 2012), ASMUS (Gross, 2012) or ENVI-met (`http://www.envi-met.com`) might help to close this knowledge gap. Also, these tools provide the opportunity to improve the understanding about underlying mechanisms of ΔT formation. Following processes contribute to urban warming compared to rural land use (Brazel & Quatrocchi, 2005):

⇒ **Net Radiation Flux ($R_n = (1-a)S_\downarrow + L_\downarrow - \varepsilon\sigma T^4 + Q_{AH}$):** Radiation absorption (positive; $S_\downarrow + L_\downarrow$) and reflection as well as emission (negative; $-aS_\downarrow$ and $-\varepsilon\sigma T^4$, respectively) of the surface are influenced by the urban geometry

⇒ **Anthropogenic Heat Flux (Q_{AH}):** Anthropogenic heat released (positive) from buildings, vehicles, metabolism and industries

⇒ **Sensible Heat Flux (Q_H):** Turbulent vertical transport (positive ↑) is reduced in an urban canopy layer

⇒ **Latent Heat Flux (Q_{LE}):** Availability of water that can evaporate (positive ↑) from vegetation or/and from other surfaces is reduced

⇒ **Storage Heat Flux (Q_S):** Heat is stored (positive, daytime) and released (negative, night) from urban building materials having higher heat capacities than rural land

and result in the surface energy balance (SEB)

$$R_n + Q_{AH} = Q_H + Q_{LE} + Q_S \tag{1}$$

for an urban neighbourhood.

When developing adaptation strategies, city planners have to quantify all the thermal impacts, which raises the question of how each of the SEB terms can be converted into its respective ΔT contribution. Micrometeorological models are based on the SEB so that ΔT contributions cannot be directly obtained from simulation results. Therefore, this paper aims at converting the energy-terms of eq. 1 into temperature differences ΔT related to the energy flux differences between rural and urban land use. We also provide an interpretation of the individual contributions to ΔT. The developed decomposition procedure of ΔT is guided by a previously suggested technique (Lee et al., 2011) on mesoscale and we demonstrate how this approach can be applied to an urban neighbourhood. In particular, our study aims to

- investigate the processes contributing to ΔT in a typical Central European mid-size city in order to improve the development of climate adaptation strategies,
- develop spatial maps for each ΔT contribution to identify areas particularly demanding for climate adaptation measures,
- analyse whether convection efficiency is also for neighbourhoods (microscale) the dominant ΔT driver as was stated for whole cities and metropolitan regions (mesoscale; Zhao et al. (2014)),
- assess how the chosen initial wind direction influences the ΔT contributions.

2. Case Study Area

The case study was realised for Leipzig, a Central European mid-size city with 595.952 inhabitants (reference: Stadt Leipzig (2018)). The city is situated in a lowland in Eastern Germany (51°20'N, 12°22'E) and classified as Cfb (warm temperate with warm summers, fully humid) climate after Köppen-Geiger (Kottek et al., 2006) with mean annual temperature 9.1 $°C$ and mean annual precipitation 584.6 mm at the German Weather Service

(DWD) station Leipzig-Holzhausen. Because of the usually dense building structure in the urban core it is very difficult to adapt such areas to climate change. A good chance for interventions arises during the planning process to revitalise urban brownfields. Leipzig has some of these areas, whereby one amongst them, the quarter around the "Bayerischer Bahnhof", was used in this study (Fig. 1). The area encompasses 455625 m^2.

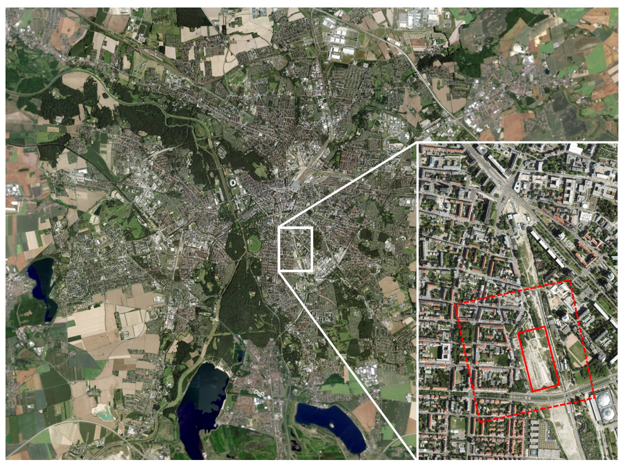

Figure 1: City region of Leipzig. The white box denotes the quarter around "Bayerischer Bahnhof"; the small red box shows a brownfield where revitalising is planned and the big red box (dashed line) characterises the simulation area which is described in section 3. (source: DOP © Staatsbetrieb Geobasisinformation und Vermessung Sachsen 2014)

3. Methodological framework

Our framework consists of a 3-step process: Firstly, we calculated the spatio-temporal development of environmental parameters by means of an **ENVI-met simulation** (version 3.1). Secondly, a procedure for the **Decomposition of ΔT** was developed and applied. Thirdly, the results were visualised and comparatively discussed.

3.1. Micrometeorological simulations for urban and rural states

ENVI-met is a 3D micrometeorological model and a state–of–the–art tool for microscale simulations (evaluated by e.g.: Yang et al., 2013; Chen et al., 2014; Elnabawi et al., 2015; Lee et al., 2016; Roth & Lim, 2017; Liu et al., 2018) with very accurate representation of microphysical processes inside the "urban boundary layer“ (e.g.: Huttner, 2012; Simon, 2016). It incorporates, fluid–mechanical, hydrological, atmospheric and thermodynamic processes. The local thermal conditions are determined through the built-up structure so that ENVI-met is particularly suitable to investigate microscale interactions between buildings, vegetation, soils and the atmospheric boundary layer. ENVI-met is classified to the group of non - hydrostatic models including, with respect to the interactions, a vegetation model and a one-dimensional soil model (Soil-Vegetation-Atmosphere-Transport (SVAT) interactions), and an atmosphere model including radiative transfer model (Bruse & Fleer, 1998).

In the past, numerous studies with ENVI-met have been undertaken but primarily about impacts of urban structures on the microclimate (e.g.: Middel et al., 2014; Skelhorn et al., 2014) and human thermal comfort (e.g.: Ali-Toudert & Mayer, 2007; Salata et al., 2015; Taleghani et al., 2015; Lee et al., 2016) as well as possible mitigation/adaptation strategies (e.g. green infrastructure: Ng et al., 2012; Zoelch et al., 2016) for urban heat reduction (Middel et al., 2014; Skelhorn et al., 2014). Although some studies incorporate UHI mitigation analyses (e.g.: Emmanuel & Fernando, 2007; O'Malley et al., 2015; Wang & Akbari, 2016) they do not consider the physical causes of ΔT formation in detail.

The characteristics of the neighbourhood simulated in our study are used as input for ENVI-met and comprise the "area-input-file“ (Tab. 1) as well as the "configuration file" (Tab. 2). To assess the impact of urban land use on ΔT, two different scenarios were simulated. The "urban state" represents the current land use and real structure of buildings in the study area. These simulations were compared with a reference scenario that is the "rural state" characterised by grassland without any urban structure. Trees, hedges and bushes remain unchanged for both scenarios.

a) "Urban state"

The neighbourhood "Bayerischer Bahnhof" was used for the ENVI-met simulations (specifications can be found in Tab. 1, visualisation in Fig. 2) and characterises the so-called "urban state". The area consists of a variety of different land use types to analyse urban impacts in detail. All land use data have been defined for each grid cell in the model area by help of a satellite image which was uploaded to the ENVI-met editor as an underlying bitmap. A cell can only be comprised of one object type (building OR vegetation) and surface type (e.g.: asphalt, concrete,...). The height of the objects is derived from a 3D urban model (Sachsen, 2012).

For our analysis, we chose a warm and cloudless day (21 July 2015) to simulate a definitive UHI effect. The output was stored during 48 h at each full hour. The first 18 h have to be considered as initialization phase after which a steady state is reached (see preliminary tests in Fig. S11 in the supplementary material). Therefore only the second day was used for the ΔT decomposition. The statistical analysis of the frequency of typical wind speeds depending on wind directions showed that high wind speeds are associated with south westerly directions and low wind speeds with easterly - south easterly directions (Fig. S12 in supplementary material). In order to cover the whole range we considered three different wind scenarios (103°-

Table 1: Specifications of the ENVI-met area input file

variable	**value**
number of grids in each dimension (x,y,z)	225,225,29
horizontal grid size	3 m x 3 m
vertical grid size	1 m
telecoping factor	20 %
starting z-level for telecoping	5 m
model rotation out of grid north	16.3°
number of nesting grids	12
soil profile nesting grids	loam
name of location	Bayerischer Bahnhof
position on earth (latitude, longitude)	51.25, 12.20
name of reference time zone	CET/UTC+1
definition longitude of time zone	15.00
geographical projection system	Gauss – Krueger

east wind, 193°- south wind and 283°- west wind) to analyse differences in ΔT contributions for typical wind directions. Since numerical models cannot calculate reliable values near their borders, an additional grid, the so called "nesting cells", was introduced outside of the modelled area. Several experiments with different numbers of nesting cells suggested that 12 cells resulted in stable simulations.

The horizontal and vertical grid sizes are constant over the core model area (Tab. 1) except the first vertical cell which is divided up into 5 single cells. The vertical grid size of the soil model is 0.015 m near the surface and up to 0.5 m in deeper layers. Boundary surfaces (roofs, walls, soils) are treated separately from the prognostic differential equations and subgrid-scale processes (microphysics) are parameterised. We selected a horizontal

Table 2: Configuration of ENVI-met (meteorological data provided by the Leipzig Institute for Meteorology)

variable	**value**
start simulation (day, time)	20.07.2015, 00:00:00
total simulation time	48 h
save model state	each 60 min
wind speed (10 m above ground)	4.0 m/s
wind direction	$103°(193°, 283°)$
roughness length at reference point	0.1
initial temperature atmosphere	293 K
specific humidity in 2500 m	5.5 g/kg
relative humidity in 2 m	38 %

grid size of 3 by 3 m and a vertical one of 1 m according to the size of the objects to be resolved (e.g. trees, streets or buildings).

To provide more realistic values for the model input, we used the ENVI-met setting of an averaged solar input. This option copies the shading effect of the built-up structure onto the nesting area, simulating the presence of a similar urban structure.

b) "Rural state"

For the reference scenario all urban structures (buildings, sealed surfaces such as asphalt or concrete) were replaced by grass representing rural conditions. Further, to get spatially constant values for the simulated parameters, they were averaged over all grid cells for each time step of the rural simulation. On the one hand such a mean rural state can not represent localised effects as for instance microscale turbulence or a homogenisation of the wind flow influencing just the local thermal characteristics. On the other hand, we achieve representative rural conditions not influenced by a subjective definition of rural model cells.

Finally, for each grid cell ΔT ensues from the temperature difference between the "urban state" simulation and the mean of the rural scenario without any urban structures.

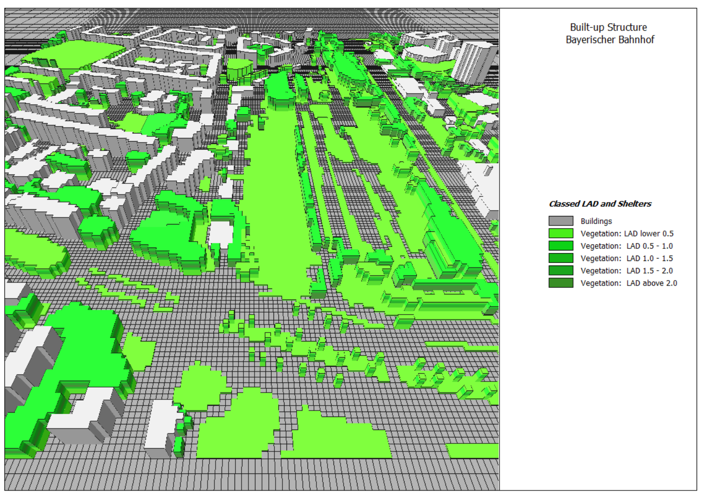

Figure 2: ENVI-met simulation area for the urban state (visualised with LEONARDO software).

3.2. Decomposition of ΔT

Here we use a decomposition approach described in detail in Hertel & Schlink (2018) and guided by Lee et al. (2011) and Zhao et al. (2014), who considered meso-(cities) and continental scales. For the neighbourhood scale we obtain a SEB (eq. 1)

$$\underbrace{(1-a)S_{\downarrow} + L_{\downarrow} - \varepsilon\sigma T^4}_{R_n} + Q_{AH} = \left(1 + \frac{1}{\beta}\right)\frac{\rho c_p}{r_a}(T - T_a) + Q_S \qquad (2)$$

(a = Albedo, $S_{\downarrow}$ = incoming short-wave radiation, $L_{\downarrow}$ = incoming long-wave radiation, ε = surface emissivity, T = surface temperature, ρ = air density, c_p = specific heat of air at constant pressure, r_a = aerodynamic resistance to heat diffusion). Q_{LE} (eq. 2) is substituted by Q_H/β involving the dimensionless Bowen ratio β.

Assuming that T_a is the temperature at a reference height, spatially constant, and not influenced by the urban structure, we can linearise the long-wave radiation term and receive

$$T - T_a = \frac{\lambda_0}{1+f}\left(R_n - Q_S + Q_{AH}\right), \tag{3}$$

with

$$f = \frac{\lambda_0 \rho c_p}{r_a}\left(1 + \frac{1}{\beta}\right), \qquad \lambda_0 = \frac{1}{4\varepsilon\sigma T_a^3}.$$

f is an energy redistribution factor and λ_0 coincides with the definition of the local climate sensitivity parameter (Roe, 2009).

Eq. 3 is applied to the temperature difference between an urban and a rural state, assuming $T \equiv T_u$ and $T_a \equiv T_r$, and using $T_u = T_r + \Delta T$ (with analogue replacements for R_n, r_a, β, Q_S and Q_{AH}; "u"-urban state, "r"-rural state). Δ represents small perturbations generated by the urban structure. Inserting these replacements into eq. 3 allows for calculating the derivatives of all quantities associated with Δ resulting in the UHI intensity (ΔT) of an urban neighbourhood. Neglecting higher order terms, it follows for ΔT

$$\Delta T \approx \underbrace{\frac{\lambda_{0,r}}{1+f_r}\Delta R_n}_{\Delta T_{R_n}} + \underbrace{\frac{-\lambda_{0,r}}{(1+f_r)^2}\left(R_{n,r} - Q_{S,r} + Q_{AH}\right)\Delta f_1}_{\Delta T_{f_1}} + \underbrace{\frac{-\lambda_{0,r}}{(1+f_r)^2}\left(R_{n,r} - Q_{S,r} + Q_{AH}\right)\Delta f_2}_{\Delta T_{f_2}} + \underbrace{\frac{-\lambda_{0,r}}{1+f_r}\Delta Q_S}_{\Delta T_{Q_S}} + \underbrace{\frac{\lambda_{0,r}}{1+f_r}\Delta Q_{AH}}_{\Delta T_{Q_{AH}}}, \tag{4}$$

with

$$\Delta f_1 = \frac{-\lambda_{0,r}\rho c_p}{r_{a,r}}\left(1+\frac{1}{\beta_r}\right)\frac{\Delta r_a}{r_{a,r}}, \qquad \Delta f_2 = \frac{-\lambda_{0,r}\rho c_p}{r_{a,r}}\frac{\Delta\beta}{\beta_r^2}.$$

All required quantities can be gathered from either the "urban simulation" output, the "rural simulation" output or in the case of physical constants from the literature (table 3). In this case study we neglected $\Delta T_{Q_{AH}}$ (Q_{AH} vanishes in all other terms) which describes the effect of anthropogenic heat and can not be calculated from ENVI-met. As the storage heat flux is not directly provided by ENVI-met, we calculated $\Delta Q_S(\mathbf{x}, t)$ applying eq. 4 to the modelled temperature difference between urban and rural simulations $\Delta T_{model} = T_u - T_r$.

$$\frac{\lambda_{0,r}}{1+f_r}\Delta Q_S \approx \frac{\lambda_{0,r}}{1+f_r}\Delta R_n + \frac{-\lambda_{0,r}}{(1+f_r)^2}\left(R_{n,r} - Q_{S,r}\right)\Delta f_1 + \frac{-\lambda_0}{(1+f)^2}\left(R_{n,r} - Q_{S,r}\right)\Delta f_2 - \Delta T_{model}, \tag{5}$$

$Q_{S,r}(\mathbf{x}, t)$ was derived as residual of the urban surface energy balance (eq. 2) for the rural state

$$Q_{S,r} = (1-a_r)S_{r\downarrow} + L_{r\downarrow} - \varepsilon_r \sigma T_r^4 - Q_{H,r} - Q_{LE,r}. \tag{6}$$

Table 3: Attribution of ENVI-met output to ΔT partitions. The overline represents spatial mean quantities.

ΔT partitions	**quantities derived from "urban simulation"**	**quantities derived from "rural simulation"**	**physical constants**
changes in radiation balance (ΔT_{R_n})	$R_{n,u}$	$\overline{R}_{n,r}\,\overline{r}_{a,r}$ $\overline{\beta}_r, \overline{\lambda}_{0,r}$	ρ, c_p
changes in convection efficiency (ΔT_{f_1})	$Q, r_{a,u}$	$\overline{R}_{n,r}, \overline{Q}_{S,r},$ $\overline{r}_{a,r}, \overline{\beta}_r, \overline{\lambda}_{0,r}$	ρ, c_p
changes in evapotranspiration (ΔT_{f_2})	Q, β_u	$\overline{R}_{n,r}, \overline{Q}_{S,r},$ $\overline{r}_{a,r}, \overline{\beta}_r, \overline{\lambda}_{0,r}$	ρ, c_p
changes in storage heat (ΔT_{Q_S})	$Q_{S,u}$	$\overline{Q}_{S,r}, \overline{r}_{a,r},$ $\overline{\beta}_r, \overline{\lambda}_{0,r}$	ρ, c_p

3.3. Visualisation

As a result of the ΔT decomposition we achieved maps of the study area for each partition of ΔT. To identify dominant contributions to urban heat and to give recommendations for local adaptation actions, the $\Delta T(\mathbf{x}, t)$'s were visualised and, for specific locations, comparatively discussed.

4. Results and discussion

The hottest surface temperature was simulated for 2 p.m., when we can expect most pronounced UHI effects (Fig. 3).

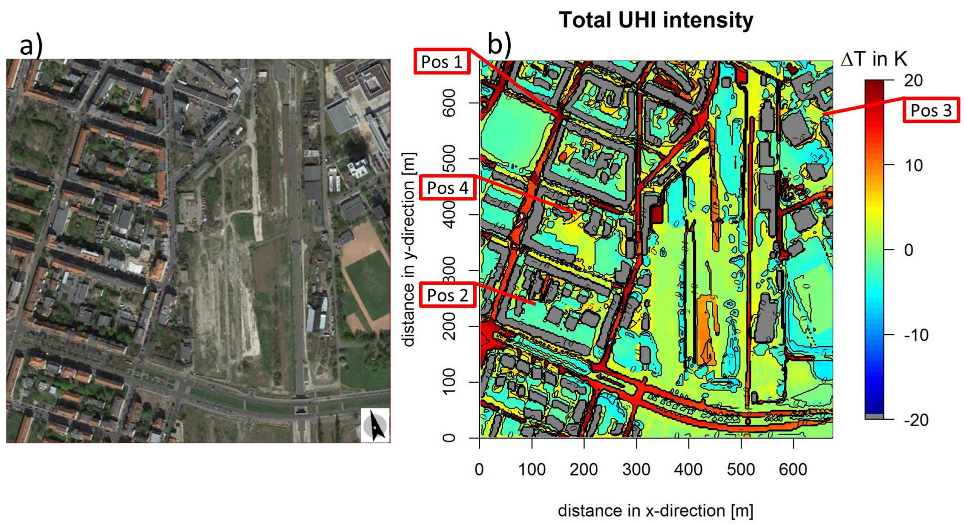

Figure 3: a) Satellite image of "Bayerischer Bahnhof" with the exact dimensions as the ENVI-met area input file (created with the "ENVI-met EagleEye v5.0" software).
b) Total UHI intensity for an east wind scenario composed from the sum of ΔT_{R_n}, ΔT_{f_1}, ΔT_{f_2} and ΔT_{Q_S} (eq. 4). Bluish contours denote cooling, reddish a warming compared with the rural state and darkgreyish buildings. The red boxes are selected locations where all contributions are discussed together in terms of adaptation opportunities (section 4.6).

4.1. Total UHI intensity: ΔT

Strong warming (reddish contours in Fig. 3b) occurs at locations without vegetation in inner courtyards, asphalt streets and most parts of the brownfield. Cooling (bluish) is mostly associated with trees, bushes/hedges and heavily shaded places. White contours (see Figs. 4 - 7) are outside the scale range and represent following critical cases.

First, if $f_r \rightarrow -1$ eq. 4 diverges and white countours are plotted in the ΔT maps. Negative values of f_r are only possible if $\beta_r < 0$ ($r_{a,r} > 0$, $\lambda_{0,r} > 0$ for physical reasons; ρ as well as c_p are positive material constants). A negative β denotes the so-called "oasis" effect where a small area evaporates more than its surroundings and this is typically found within a desert or over lakes. Warm and dry air flows over a very wet surface resulting in a large latent heat flux directed upwards to the atmosphere. This evaporation cools the surface and generates a sensible heat flux directed downwards. To a lesser extent such a phenomenon can be found near single trees, small vegetated areas or irrigated surfaces surrounded by very dry areas (e.g. sealed surfaces).

Second, if $Q_{LE} \rightarrow 0$, which happens quite often over dry surfaces, β becomes very large. As a result, Δf_2 becomes very small, f_r very large and so especially ΔT_{f_2} would be close to 0 which looks like a "0 contour" in Fig. 6 and cannot be resolved. This goes along with areas where no or less evapotranspiration take place. Often, this is the case over, e.g., urbanised regions with a high percentage of impervious soils and especially at night due to the absence of solar radiation.

Third, for $r_a \rightarrow 0$ and/or $\beta \rightarrow 0$, f_r, Δf_1 and Δf_2 give infinite solutions ("poles"). As a result, $\Delta T \rightarrow 0$.

4.2. Changes in radiation balance: ΔT_{R_n}

The temperature increase arising from the radiation balance (Fig. 4) responds to shading effects of buildings and vegetation. Shading within vegetation is primarily determined by the leaf area density (LAD). Therefore, greatest cooling was found under very dense tree crowns and hedges, especially within inner courtyards (e.g. Fig. 4 left side, residential area) and next to high buildings. A slight warming occurs at concrete surfaces (e.g. main

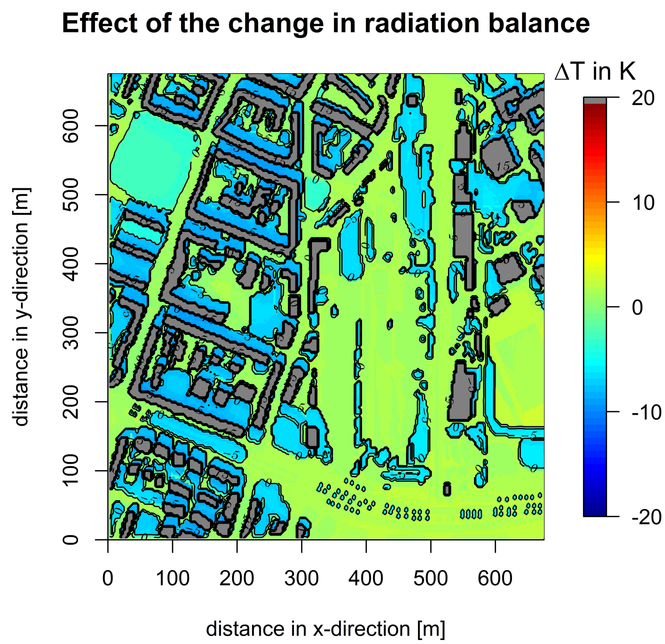

Figure 4: ΔT_{R_n} caused by changes in the radiation balance. Colours are the same as in Fig. 3b. The simulation was done for an east wind scenario.

road in the south of the brownfield) which can absorb more short-wave radiation than natural surfaces. Asphalt and the open built-up structure causes a warming although, as soon as the road reaches a narrow street canyon in the residential area, shadowing is created by the surrounding buildings. Due to sun height (53.23°) and azimuth angle (206.39°), preferably radiation can laterally penetrate into south-north oriented street canyons and produces a surplus of heat (shadows in Fig. 3a indicate the sun position).

The wind direction slightly modifies ΔT_{R_n} since turbulent fluxes are determined by the flow field and are incorporated in f. Differences occur in the magnitude of both warming and cooling while the principal patterns are the same. South as well as west wind scenarios (in supplementary material Figs. S1 and S6, respectively) are only a few hundredth till tenths of a degree cooler or warmer than the east wind scenario.

4.3. Changes in convection efficiency: ΔT_{f_1}

Zhao et al. (2014) observed that, in humid climate zones, convection efficiency in cities was lower (r_a higher) than in their rural surroundings. This is likewise valid for Leipzig in temperate climate (Fig. 5). Convection efficiency slightly depends on the wind scenario and the built-up structure. For example, in the residential area on the left side in Fig. 5 there is a SSW - NNE oriented street affected by cooling. The same street shows a slight warming under south wind conditions (Fig. S2 in supplementary material) and a change between warming and cooling under west wind conditions (Fig. S7 in supplementary material) due to the nature of convection efficiency. The higher r_a the more turbulence with tendency to small eddies can be produced. In contrast, in the rural area without any buildings turbulence produces larger convection cells and therefore r_a is reduced. Large eddies are more effective in removing heat from the surface than smaller ones.

Under east wind conditions the flow field is nearly perpendicular oriented to the buildings along the above considered street and this causes lee eddies inside the street canyon. In the south and west wind scenario the orientation of the obstacles is more various which causes more small eddies. This reduces the heat removing efficiency which in turn ends up in warming. Besides building orientation also the wind speed controls the convection efficiency since r_a (interpreted as resistance of the interface against the temperature gradient) decreases with increasing wind speed because of enhanced

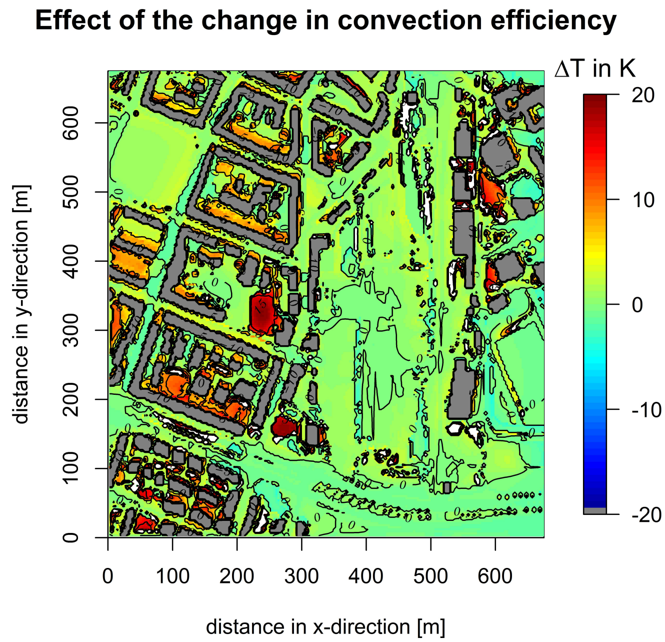

Figure 5: same as Fig. 4 but for ΔT_{f_1} due to convection efficiency

mixing of air masses. The lower r_a the higher Q_H resulting in a higher heat removing efficiency. In case of channelling effects between buildings or no blocking obstacles in wind direction, the wind speed is high and causes cooling. For instance, near some objects and street canyons directly behind the inflow edge the flow is slowed but, on the other hand, accelerated within the canyons. The shape and dimension of the cooling contours depend on these effects which can be seen by comparing the three wind scenarios (Figs. 5, S2 and S7 in supplementary material). Anyway, the temperature differences are very small and again the spatial patterns are quite similar.

4.4. Changes in evapotranspiration: ΔT_{f_2}

Evapotranspiration is restricted to vegetation and unsealed surfaces. Sealed surfaces are impervious to water. Therefore at, e.g., asphalt roads, concrete surfaces and buildings, no value can be calculated by the decomposition scheme described (darkgrey contours in Fig. 6).

The transpiration of vegetation depends on the LAD and, consequently, the greatest cooling effect can be identified in the surrounding of trees with very dense crowns and hedges with high LAD. Sand surfaces (e.g. around a

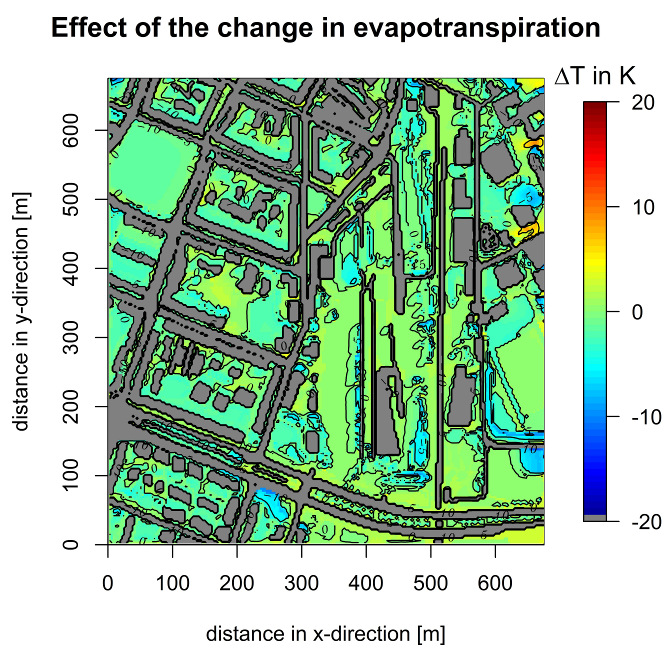

Figure 6: same as Fig. 4 but for ΔT_{f_2} due to evapotranspiration (darkgreyish contours denote buildings and sealed surfaces).

sports ground), as used in ENVI-met, are situated above wet soil resulting in a constant humidity; and since such a soil type is very pervious to water it produces strong cooling (Fig. 6). The propagation of the cooling effect into surrounding cells depends on wind direction and turbulent humidity transport. Places with a strong cooling behind the respective inflow edge are warmer for another wind scenario.

Warming due to ΔT_{f_2} is dominated by surfaces with low percentage of dense vegetation. Only a few scrubs and bushes or grass (see brownfield) are situated at such locations. Often, e.g. in inner courtyards, vegetation is completely missing. In total, the differences are small ($\approx \pm 1K$).

4.5. Changes in storage heat: ΔT_{Q_S}

Over annual periods the average storage heat flux vanishes. For our study with a temporal resolution of 1 hour the storage heat can reach significant magnitudes. The amount of stored heat primarily depends on the

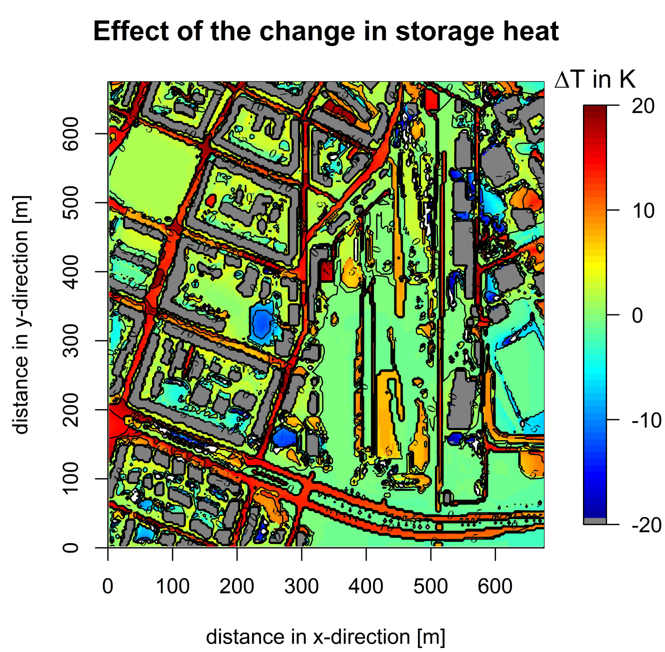

Figure 7: same as Fig. 4 but for ΔT_{Q_S} due to storage heat

surface material and its specific heat capacity. Thus, e.g., asphalt roads show a strong warming (Fig. 7) while most vegetated areas, loamy and sandy soils in the brownfield or around the sports ground are cool.

The warming within some tree groups (e.g. right inflow edge, south of the sports ground in Fig. 7) is somewhat surprising. Cool air produced above vegetation canopies (e.g. tree crowns) can sink downwards because of its higher density and mix up with the underlying warmer air masses. The denser the vegetation is, the more heat can be stored under the vegetation canopy and can be used for mixing with cold air. For that reason the "canopy surface" can be seen warmer than one would expect and creates a warming compared with the rural state.

The propagation of warming or cooling effects into surrounding cells depends on the wind direction where the strongest warming can be found in the main streets under east and west wind conditions (Figs. 7 and S5 in supplementary material).

4.6. Decomposition of ΔT at selected locations

As a check of plausibility of the decomposition procedure we discuss the individual UHI contributions at four exemplary positions (Table 4, locations marked in Fig. 3b).

At location 1 there is a hot spot ($\Delta T = +19.2$ K). The dominant driver with ≈ 18.4 K is storage heat due to high heat capacity of the asphalt surface. Although this place is surrounded by buildings, a radiation surplus leads to a slightly positive UHI contribution ($\Delta T_{R_n} \approx +0.7$ K). According to the sun position (paragraph 4.2) shading is not effective since a street is crossing this place from south west to north east. Because of scattering at surrounding objects, this orientation allows for more radiation reaching the surface compared to the rural state. The sky-view factor is higher (0.65) than for position 2 and 4. For cooling more shading is desirable. Because of an impervious asphalt surface, evaporation is negligible ($\Delta T_{f_2} = 0$). As a consequence, at location 1 an adequate strategy for climate adaptation would be to enable evaporation, e.g. by using pervious asphalt materials (e.g. with organic binding materials) or by unsealed surfaces. Additionally, this would reduce the large contribution to ΔT_{Q_S}.

Location 2 is situated inside a courtyard under tree crowns which produce cooling ($\Delta T = -2.9$ K). Both the shadow and enhanced transpiration of vegetation are responsible for that ($\Delta T_{R_n} < 0, \Delta T_{f_2} < 0$) and the sky-view factor has by far the lowest value (0.01). Nearly the complete sky is obstructed. Convection is inefficient and provides the most dominant contribution ($\Delta T_{f_1} \approx 15.7$ K) because of low wind speed inside the courtyards and a small Q_H ($\approx 5.4\ W/m^2$). The other processes overcompensate this effect so that, nevertheless, cooling develops. This example highlights how cooling can be achieved in a dense urban quarter and that it is, a priori, not obvious which contribution is dominant. This requires detailed investigation.

Location 3 is in a schoolyard with loamy soil and shows slight warming. Interestingly, here the convection efficiency is increased and causes cooling ($\Delta T_{f_1} \approx -2$ K). The schoolyard is not completely enclosed with buildings so that the wind can flow undisturbed through the area (high wind speed).

The dominant contribution to warming is the lack of evapotranspiration as the entire schoolyard has no or less vegetation ($\Delta T_{f_2} \approx +8.8$ K). Although this place has an open space characteristic (sky-view factor = 0.66 is highest), radiation plays only a minor role due to shadowing by buildings. This discussion highlights the strengths of the described approach in order to decide which adaptation measure is feasible in terms of a cost–benefit assessment. At this specific location it is clearly recommendable using irrigated grass surfaces. On the one hand, they can reduce surface temperatures and on the other hand pupils could use these areas for relaxing, talking and playing with their friends during summertime.

Location 4 shows warming. Because of the position next to a building, inside a courtyard and without vegetation all contributions provide a warming (even radiation because of the sun position (although the sky-view factor is relatively high (0.57)); see section 4.2). The dominant contribution is ΔT_{Q_S} with ≈ 3.3 K. The best option at this location is irrigated grass to enhance evapotranspiration and to increase albedo that reduces radiation absorption and the resulting stored heat. For instance, the 2-m air temperature at daytime can be reduced by up to 4 K (Morini et al., 2018) within single neighbourhoods and on average 0.8 and 0.4 K at urban/rural areas (Jandaghian & Akbari, 2018), respectively. It is to be expected that the reduction for the surface temperature will be even more pronounced.

Table 4: Total ΔT and its contributions at 4 locations in the quarter including sky-view factor.

position	$\boldsymbol{\Delta T}$ **[K]**	$\boldsymbol{\Delta T_{R_n}}$ **[K]**	$\boldsymbol{\Delta T_{f_1}}$ **[K]**	$\boldsymbol{\Delta T_{f_2}}$ **[K]**	$\boldsymbol{\Delta T_{Q_S}}$ **[K]**	**sky-view factor**
1 (junction)	19.2	0.7	0.1	0	18.4	0.65
2 (courtyard)	-2.9	-6.8	15.7	-2.6	-9.2	0.01
3 (schoolyard)	2.4	0.9	-2.0	8.8	-5.3	0.66
4 (near building)	6.5	0.6	1.3	1.3	3.3	0.57

5. Limitations

225 by 225 cells were available for the simulation. To get reasonable results and to include local structures (e.g. streets or single trees) a grid size smaller than 5 by 5 m is needed to dissolve such small objects, which are important for the local UHI formation. This limits the possible modelling area to approx. 1125 by 1125 m.

Local heat occurs mainly in an autochthonous weather situation as we assumed in our study. To simulate this stable atmosphere, initial wind speed was low (4 m/s). This might cause inaccurate simulations.

Generally, UHI intensity is strongly affected by the surface material. Since flux divergences (e.g.: radiation) from surrounding cells into the actual model cell are not taken into account by the present approach, the transitions between contours are quite sharp.

An additional restriction is that, although ENVI-met (version 3) considers shadows for radiation calculation, inclination and exposition of surfaces are not included. Anthropogenic heat was neglected but studies like Ichinose et al. (1999) showed that anthropogenic heat at high resolutions can reach 800 W/m^2 (downtown Tokyo) which is why future modelling approaches should incorporate such fluxes. Since anthropogenic heat is originally involved in ΔT_{f_1} and ΔT_{f_2}, only their magnitudes can be influenced but not the principal spatial patterns. Another issue are large values of the Bowen ratio β through $Q_{LE} \rightarrow 0$. This problem cannot be neglected at the neighbourhood scale (grid size within a few metres).

6. Conclusions

We suggested an approach for the decomposition of urban warming ΔT and applied it to a neighbourhood in Leipzig, Germany. The resulting maps of the individual UHI contributions as well as their discussion at places of interest demonstrated that:

- There is no overall dominating UHI contribution; nevertheless storage heat and convection efficiency dominate most parts of the quarter.
- The greatest warming was found in streets with no or less trees, over impervious surfaces such as asphalt or concrete and in general over unshaded areas with no or less vegetation (brownfield, parts of inner courtyards and street canyons).
- Convection efficiency (that was previously presumed to be responsible for UHI in humid climates (Zhao et al., 2014)) proved to be not always the dominant driver for local UHI intensity. Often storage heat contributes the most to UHI.
- The dynamical production of turbulent kinetic energy (TKE) and their dissipation is highly influenced by wind speed and direction which in turn depends on the orientation of obstacles within the flow field. Therefore, the convection efficiency slightly differs for the three wind scenarios (east, south, west). Pronounced differences were found for the storage heat where east and west wind scenarios showed the strongest warming effect. For the south wind scenario the warming at most areas is considerably smaller but in a few streets perpendicular to the wind direction it is stronger.

Our study demonstrated that this approach can be a valuable contribution for a targeted development of mitigation and adaptation strategies to urban climate change.

7. Software and technical notes

For micrometeorological simulations the model ENVI-met (`http://www.envi-met.com/`) was used. To avoid inconsistencies in the results by using different model versions we used version 3.1 for all applications. Input data are achieved from a 3D city model (buildings; Sachsen (2012)) and a meteorological measurement site (Institute for Meteorology – Leipzig; data: `http://meteo.physgeo.uni-leipzig.de/de/wetterdaten/index.php`). Visualisation, conversion of ENVI-met output data (from binary format), decomposition of ΔT and the analysis were done with programs developed in R (R Core Team, 2015). The code also implements eq. 4 - 6 and is available on request from the authors.

Acknowledgments

D. H. was financially supported by the Deutsche Bundesstiftung Umwelt DBU (German Federal Environmental Foundation), Osnabrück.

References

Ali-Toudert, F., & Mayer, H. (2007). Effects of asymmetry, galleries, overhanging facades and vegetation on thermal comfort in urban street canyons. *SOLAR ENERGY*, *81*, 742–754. doi:{10.1016/j.solener.2006.10.007}.

Arnfield, A. (2003). Two decades of urban climate research: A review of turbulence, exchanges of energy and water, and the urban heat island. *INTERNATIONAL JOURNAL OF CLIMATOLOGY*, *23*, 1–26. doi:10.1002/joc.859.

Brazel, A., & Quatrocchi, D. (2005). Urban Climatology . In Oliver, J.E. (Ed.), *Encyclopedia of World Climatology* chapter 219. (pp. 766–779). Dordrecht: Springer Netherlands. doi:10.1007/1-4020-3266-8_219.

Bruse, M., & Fleer, H. (1998). Simulating surface-plant-air interactions inside urban environments with a three dimensional numerical model. *ENVIRONMENTAL MODELLING & SOFTWARE*, *13*, 373–384. doi:10.1016/S1364-8152(98)00042-5.

Chen, Y.-C., Lin, T.-P., & Matzarakis, A. (2014). Comparison of mean radiant temperature from field experiment and modelling: a case study in Freiburg, Germany. *THEORETICAL AND APPLIED CLIMATOLOGY*, *118*, 535–551. doi:{10.1007/s00704-013-1081-z}.

Christidis, N., Jones, G. S., & Stott, P. A. (2015). Dramatically increasing chance of extremely hot summers since the 2003 European heatwave. *NATURE CLIMATE CHANGE*, *5*, 46–50. doi:{10.1038/NCLIMATE2468}.

Eichhorn, J. (2011). *MISKAM: Handbuch zu Version 6*. URL: http://www.lohmeyer.de/de/system/files/content/download/software/HB_MISKAM.pdf.

Elnabawi, M. H., Hamza, N., & Dudek, S. (2015). Numerical modelling evaluation for the microclimate of an outdoor urban form in Cairo, Egypt. *HBRC Journal*, *11*, 246 – 251. URL: http://www.sciencedirect.com/science/article/pii/S168740481400025X. doi:{https://doi.org/10.1016/j.hbrcj.2014.03.004}.

Emmanuel, R., & Fernando, H. J. S. (2007). Urban heat islands in humid and arid climates: role of urban form and thermal properties in Colombo, Sri Lanka and Phoenix, USA. *CLIMATE RESEARCH*, *34*, 241–251. doi:{10.3354/cr00694}.

Grimmond, C., & Oke, T. (2002). Turbulent heat fluxes in urban areas: Observations and a local-scale urban meteorological parameterization scheme (LUMPS). *JOURNAL OF APPLIED METEOROLOGY*, *41*, 792–810. doi:10.1175/1520-0450(2002)041<0792:THFIUA>2.0.CO;2.

Gross, G. (2012). Effects of different vegetation on temperature in an urban building environment. Micro-scale numerical experiments. *METEOROLOGISCHE ZEITSCHRIFT*, *21*, 399–412. doi:10.1127/0941-2948/2012/0363.

Hertel, D., & Schlink, U. (2018). How to convert urban energy balance into contributions to urban excess temperatures? submitted to MethodsX.

Holmer, B., & Eliasson, I. (1999). Urban-rural vapour pressure differences and their role in the development of urban heat islands. *INTERNATIONAL JOURNAL OF CLIMATOLOGY*, *19*, 989–1009. doi:10.1002/(SICI)1097-0088(199907)19:9<989::AID-JOC410>3.0.CO;2-1.

Huttner, S. (2012). *Further development and application of the 3D microcli-*

mate simulation ENVI-met. Ph.D. thesis Johannes Gutenberg University Mainz.

Ichinose, T., Shimodozono, K., & Hanaki, K. (1999). Impact of anthropogenic heat on urban climate in Tokyo. *ATMOSPHERIC ENVIRONMENT*, *33*, 3897–3909. doi:10.1016/S1352-2310(99)00132-6. International Conference on Urban Climatology (ICUC 96), ESSEN, GERMANY, JUN 10, 1996-JUN 14, 1997.

Jandaghian, Z., & Akbari, H. (2018). The effects of increasing surface reflectivity on heat-related mortality in greater montreal area, canada. *Urban Climate*, *25*, 135 – 151. URL: http://www.sciencedirect.com/science/article/pii/S2212095518301160. doi:https://doi.org/10.1016/j.uclim.2018.06.002.

Kottek, M., Grieser, J., Beck, C., Rudolf, B., & Rubel, F. (2006). World map of the Köppen-Geiger climate classification updated. *METEOROLOGISCHE ZEITSCHRIFT*, *15*, 259–263. URL: http://dx.doi.org/10.1127/0941-2948/2006/0130. doi:{10.1127/0941-2948/2006/0130}.

Kuttler, W., Weber, S., Schonnefeld, J., & Hesselschwerdt, A. (2007). Urban/rural atmospheric water vapour pressure differences and urban moisture excess in Krefeld, Germany. *INTERNATIONAL JOURNAL OF CLIMATOLOGY*, *27*, 2005–2015. doi:10.1002/joc.1558. 6th International Conference for Urban Climate (ICUC6), Goteborg, SWEDEN, JUN 12-16, 2006.

Lee, D. (1991). URBAN RURAL HUMIDITY DIFFERENCES IN LONDON. *INTERNATIONAL JOURNAL OF CLIMATOLOGY*, *11*, 577–582.

Lee, H., Mayer, H., & Chen, L. (2016). Contribution of trees and grasslands to the mitigation of human heat stress in a residential district of Freiburg, Southwest Germany. *LANDSCAPE AND URBAN PLANNING*, *148*, 37–50. doi:{10.1016/j.landurbplan.2015.12.004}.

Lee, X., Goulden, M. L., Hollinger, D. Y., Barr, A., Black, T. A., Bohrer, G., Bracho, R., Drake, B., Goldstein, A., Gu, L., Katul, G., Kolb, T., Law, B. E., Margolis, H., Meyers, T., Monson, R., Munger, W., Oren, R., U, K. T. P., Richardson, A. D., Schmid, H. P., Staebler, R., Wofsy, S., & Zhao, L. (2011). Observed increase in local cooling effect of deforestation at higher latitudes. *NATURE*, *479*, 384–387. doi:10.1038/nature10588.

Liu, Z., Zheng, S., & Zhao, L. (2018). Evaluation of the envi-met vegetation model of four common tree species in a subtropical hot-humid area. *Atmosphere*, *9*. URL: http://www.mdpi.com/2073-4433/9/5/198. doi:10.3390/atmos9050198.

Middel, A., Haeb, K., Brazel, A. J., Martin, C. A., & Guhathakurta, S. (2014). Impact of urban form and design on mid-afternoon microclimate in Phoenix Local Climate Zones. *LANDSCAPE AND URBAN PLANNING*, *122*, 16–28. doi:{10.1016/j.landurbplan.2013.11.004}.

Morabito, M., Crisci, A., Messeri, A., Messeri, G., Betti, G., Orlandini, S., Raschi, A., & Maracchi, G. (2017). Increasing Heatwave Hazards in the Southeastern European Union Capitals. *Atmosphere*, *8*. URL: http://www.mdpi.com/2073-4433/8/7/115. doi:{10.3390/atmos8070115}.

Morini, E., Touchaei, A. G., Rossi, F., Cotana, F., & Akbari, H. (2018). Evaluation of albedo enhancement to mitigate impacts of urban heat island in rome (italy) using wrf meteorological model. *Ur-*

ban Climate, *24*, 551 – 566. URL: http://www.sciencedirect.com/science/article/pii/S2212095517300652. doi:https://doi.org/10.1016/j.uclim.2017.08.001.

Ng, E., Chen, L., Wang, Y., & Yuan, C. (2012). A study on the cooling effects of greening in a high-density city: An experience from Hong Kong. *BUILDING AND ENVIRONMENT*, *47*, 256–271. doi:{10.1016/j.buildenv.2011.07.014}.

O'Malley, C., Piroozfar, P., Farr, E. R. P., & Pomponi, F. (2015). Urban Heat Island (UHI) mitigating strategies: A case-based comparative analysis. *SUSTAINABLE CITIES AND SOCIETY*, *19*, 222–235. doi:{10.1016/j.scs.2015.05.009}.

R Core Team (2015). *R: A Language and Environment for Statistical Computing*. R Foundation for Statistical Computing Vienna, Austria. URL: https://www.R-project.org/.

Roe, G. (2009). Feedbacks, timescales, and seeing red. *Annual Review of Earth and Planetary Sciences*, *37*, 93–115. URL: https://doi.org/10.1146/annurev.earth.061008.134734. doi:10.1146/annurev.earth.061008.134734. arXiv:https://doi.org/10.1146/annurev.earth.061008.134734.

Roth, M. (2000). Review of atmospheric turbulence over cities. *QUARTERLY JOURNAL OF THE ROYAL METEOROLOGICAL SOCIETY*, *126*, 941–990. doi:10.1256/smsqj.56408.

Roth, M., & Lim, V. H. (2017). Evaluation of canopy-layer air and mean radiant temperature simulations by a microclimate model over a tropical residential neighbourhood. *BUILDING AND ENVIRONMENT*, *112*, 177–189. doi:{10.1016/j.buildenv.2016.11.026}.

Sachsen (2012). 3D-Stadtmodell© Staatsbetrieb Geobasisinformation und Vermessung Sachsen.

Sailor, D. J. (2011). A review of methods for estimating anthropogenic heat and moisture emissions in the urban environment. *INTERNATIONAL JOURNAL OF CLIMATOLOGY*, *31*, 189–199. doi:10.1002/joc.2106. 7th International Conference on Urban Climate (ICUC-7), Yokohama, JAPAN, JUN 29-JUL 03, 2009.

Salata, F., Golasi, I., Vollaro, E. d. L., Bisegna, F., Nardecchia, F., Coppi, M., Gugliermetti, F., & Vollaro, A. d. L. (2015). Evaluation of Different Urban Microclimate Mitigation Strategies through a PMV Analysis. *SUSTAINABILITY*, *7*, 9012–9030. doi:{10.3390/su7079012}.

Sievers, U. (2012). *Das kleinskalige Strömungsmodell MUKLIMO. Teil 1: Theoretische Grundlagen, PC-Basisversion und Validierung.* volume 240 of *Berichte des DWD*. Offenbach am Main: Selbstverlag des Deutschen Wetterdienstes.

Sievers, U., & Zdunkowski, W. (1986). A microscale urban climate model. *CONTRIBUTIONS TO ATMOSPHERIC PHYSICS*, *59*, 13–40.

Simon, H. (2016). *Modeling urban microclimate - Development, implementation and evaluation of new and improved calculation methods for the urban microclimate model ENVI-met*. Ph.D. thesis Johannes Gutenberg University Mainz.

Skelhorn, C., Lindley, S., & Levermore, G. (2014). The impact of vegetation types on air and surface temperatures in a temperate city: A fine scale assessment in Manchester, UK. *LANDSCAPE AND URBAN PLANNING*, *121*, 129–140. doi:{10.1016/j.landurbplan.2013.09.012}.

Stadt Leipzig, Amt für Statistik und Wahlen. (2018). "Wohnberechtigte Einwohner (Registerdaten)". https://statistik.leipzig.de/statcity/table.aspx?cat=2&rub=4&per=q. [Online; accessed March 27, 2018].

Taleghani, M., Kleerekoper, L., Tenpierik, M., & van den Dobbelsteen, A. (2015). Outdoor thermal comfort within five different urban forms in the Netherlands. *BUILDING AND ENVIRONMENT*, *83*, 65–78. doi:{10.1016/j.buildenv.2014.03.014}.

Wang, Y., & Akbari, H. (2016). Analysis of urban heat island phenomenon and mitigation solutions evaluation for Montreal. *SUSTAINABLE CITIES AND SOCIETY*, *26*, 438–446. doi:{10.1016/j.scs.2016.04.015}.

Yang, X., Zhao, L., Bruse, M., & Meng, Q. (2013). Evaluation of a microclimate model for predicting the thermal behavior of different ground surfaces. *BUILDING AND ENVIRONMENT*, *60*, 93–104. doi:{10.1016/j.buildenv.2012.11.008}.

Zhao, L., Lee, X., Smith, R. B., & Oleson, K. (2014). Strong contributions of local background climate to urban heat islands. *NATURE*, *511*, 216–219. doi:10.1038/nature13462.

Zoelch, T., Maderspacher, J., Wamsler, C., & Pauleit, S. (2016). Using green infrastructure for urban climate-proofing: An evaluation of heat mitigation measures at the micro-scale. *URBAN FORESTRY & URBAN GREENING*, *20*, 305–316. doi:{10.1016/j.ufug.2016.09.011}.